

A Robust Real-Time Lane Detection Method with Fog-Enhanced Feature Fusion for Foggy Conditions

Ronghui Zhang^a, Yuhang Ma^a, Tengfei Li^a, Ziyu Lin^a, Yueying Wu^a, Junzhou Chen^{a,*}, Lin Zhang^b, Jia Hu^c, Tony Z. Qiu^d, Konghui Guo^e

^aGuangdong Key Laboratory of Intelligent Transportation System, School of Intelligent Systems Engineering, Sun Yat-sen University, Guangzhou, 510275, China

^bCollege of Automotive Studies, Tongji University, Shanghai, 201804, China

^cCollege of Transportation Engineering, Tongji University, Shanghai, 201804, China

^dDepartment of Civil and Environmental Engineering, University of Alberta, Edmonton, Alberta, Canada

^eState Key Laboratory of Automotive Chassis Integration and Bionics, Jilin University, Changchun, 130025, China

Abstract

Lane detection is a critical component of Advanced Driver Assistance Systems (ADAS). Existing lane detection algorithms generally perform well under favorable weather conditions. However, their performance degrades significantly in adverse conditions, such as fog, which increases the risk of traffic accidents. This challenge is compounded by the lack of specialized datasets and methods designed for foggy environments. To address this, we introduce the FoggyLane dataset, captured in real-world foggy scenarios, and synthesize two additional datasets, FoggyCULane and FoggyTusimple, from existing popular lane detection datasets. Furthermore, we propose a robust Fog-Enhanced Network for lane detection, incorporating a Global Feature Fusion Module (GFFM) to capture global relationships in foggy images, a Kernel Feature Fusion Module (KFFM) to model the structural and positional relationships of lane instances, and a Low-level Edge Enhanced Module (LEEM) to address missing edge details in foggy conditions. Comprehensive experiments demonstrate that our method achieves state-of-the-art performance, with F1-scores of 95.04 on FoggyLane, 79.85 on FoggyCULane, and 96.95 on FoggyTusimple. Additionally, with TensorRT acceleration, the method reaches a processing speed of 38.4 FPS on the NVIDIA Jetson AGX Orin, confirming its real-time capabilities and robustness in foggy environments.

Keywords: ADAS, Intelligent vehicle, Foggy lane detection dataset, Foggy lane detection, Global attention, Edge enhancement

1. Introduction

Lane detection plays an important role in Advanced Driver Assistance Systems (ADAS), providing essential support for lane keeping, autonomous navigation, and lane departure warnings, which help reduce the risk of lane-deviation accidents. As intelligent driving technologies advance, the need for robust and real-time lane

detection in complex road environments is becoming more apparent, making it a key research focus in autonomous driving (Chen et al., 2026).

Under good weather and clear lane markings, current lane detection algorithms perform well. However, in complex road environments and poor weather, such as those with poor weather conditions like fog, lane markings can become blurred, image quality may decrease, and global environmental information is often obscured, which makes lane detection more challenging (Sang and Norris, 2025). In these conditions, existing algorithms often struggle and may fail, leading to an increased risk of traffic accidents with more severe consequences. Ensuring safe driving in these conditions calls for the development of high-precision, highly robust lane detection methods optimized for foggy environments. As shown in Fig. 1, the in-vehicle camera

*Corresponding author

Email addresses: zhangrh25@mail.sysu.edu.cn (Ronghui Zhang), mayh39@mail2.sysu.edu.cn (Yuhang Ma), litf23@mail2.sysu.edu.cn (Tengfei Li), linzy88@mail2.sysu.edu.cn (Ziyu Lin), wuyy236@mail2.sysu.edu.cn (Yueying Wu), chenjunzhou@mail.sysu.edu.cn (Junzhou Chen), tongjizl@tongji.edu.cn (Lin Zhang), hujia@tongji.edu.cn (Jia Hu), zhijunqiu@ualberta.ca (Tony Z. Qiu), guokh@jlu.edu.cn (Konghui Guo)

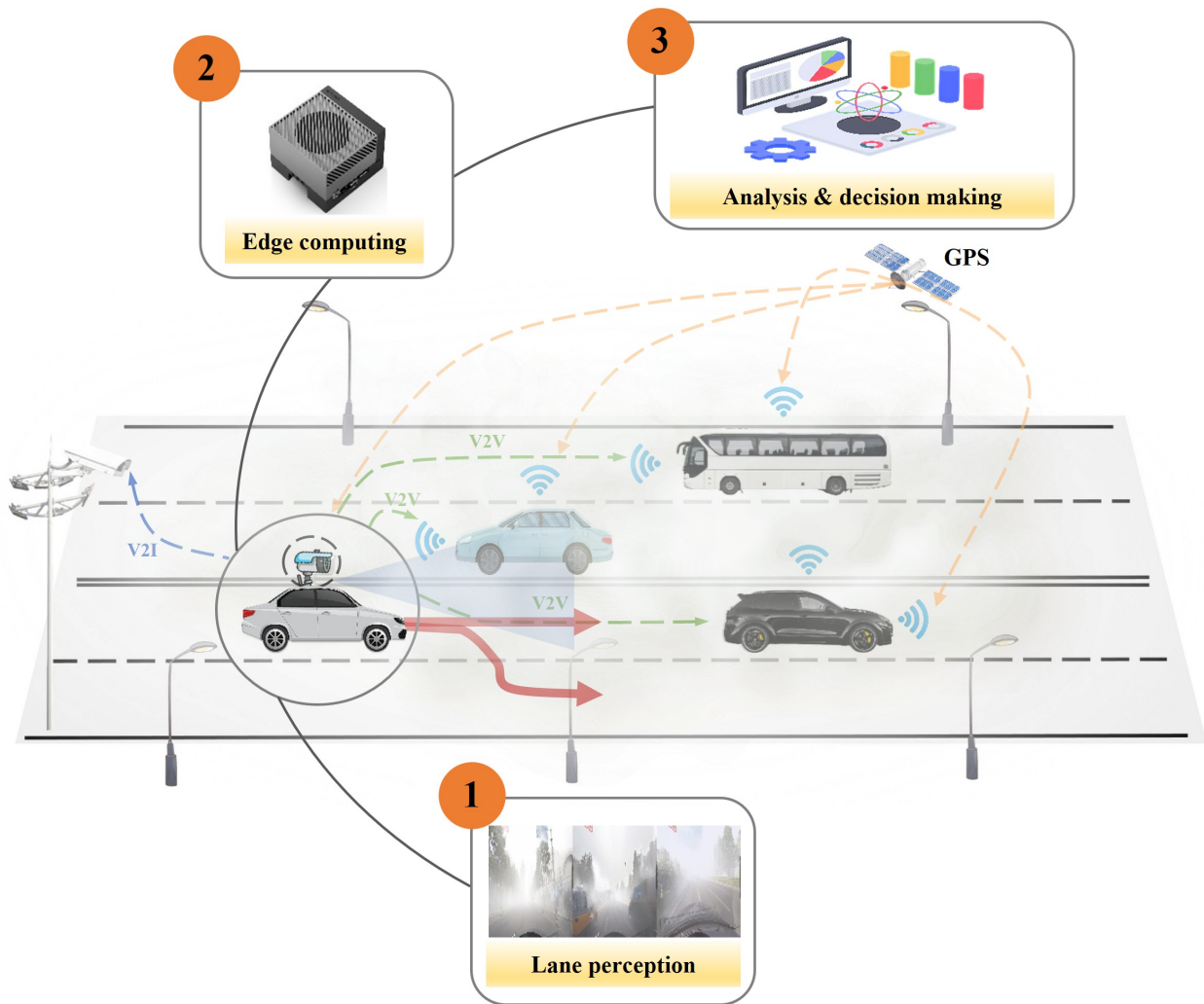


Figure 1: Lane detection in foggy scenarios for ADAS.(Pexels, 2025)

captures real-time road images, which are preprocessed by edge devices and then sent to the lane detection module. Detected lane information is fused with data from other sensors, such as radar and GPS, along with real-time traffic data from the cloud. This information is processed in the vehicle's computing unit, allowing the system to make adaptive driving decisions—such as accelerating, braking, or steering—to ensure safety in challenging environments like fog.

Although end-to-end autonomous driving technologies have made significant progress at Level 3 (L3) and higher, most current vehicles, particularly commercial and urban vehicles, are still at Level 0 (L0), Level 1 (L1), and Level 2 (L2). In these lower levels of autonomous driving, lane detection remains a crucial technology, especially in complex and adverse road envi-

ronments. Most existing vehicles rely on Advanced Driver Assistance Systems (ADAS) to enhance safety in complex scenarios, especially in active warning, lane-keeping, and other functions. For example, Zhang and Zhu (2019) proposed an autonomous path tracking control method for intelligent electric vehicles based on lane detection and an optimal preview strategy, demonstrating that accurate lane recognition and trajectory tracking are fundamental to ensuring driving stability and safety at lower automation levels (Zhang and Zhu, 2019). Similarly, recent research highlights that coordinated lane-changing strategies in mixed traffic, such as the decentralized multi-vehicle decision-making framework developed by Alshakhs et al., are essential for improving both traffic efficiency and safety in environments where human-driven vehicles and connected au-

tomated vehicles coexist (Alshakhs et al., 2025). Therefore, this research not only focuses on end-to-end autonomous driving technologies but also aims to improve lane detection performance in complex environments, providing stronger safety support and driving assistance for L0, L1, and L2 vehicles in adverse conditions.

Earlier lane detection algorithms mainly relied on traditional computer vision methods. Son et al. (Son et al., 2015) first detected the vanishing point to select the ROI adaptively, then extracted lane markings based on color features and performed clustering. Hou et al. (Hou et al., 2016) used the Canny operator for edge detection and applied a progressive probabilistic Hough transform to detect lines. While these feature-based methods are efficient and suitable for real-time applications, they require manual parameter tuning and struggle in challenging conditions such as worn or occluded lane markings.

With deep learning’s success in many traffic tasks (Zhang et al., 2024b; Shunmuga Perumal et al., 2023; Preeti and Rana, 2024; Awan et al., 2025), it has become the mainstream approach for lane detection due to its strong feature extraction capabilities and better generalization. Deep learning offers higher robustness, adapting well to complex road environments and handling missing or occluded lane markings (Neven et al., 2018; Abualsaud et al., 2021; Yu et al., 2018; Pan et al., 2018). However, many networks rely on pixel-by-pixel classification, whereas lane detection does not require dense pixel segmentation. Qin et al. (Qin et al., 2020) addressed this by reframing lane detection as a row-based segmentation problem, reducing computational cost and improving detection speed.

In addition to segmentation methods, lane detection also includes detection-based approaches, many borrowing Anchor-based methods from object detection (Redmon, 2016; Farhadi and Redmon, 2018). Due to the elongated shape of lane lines, traditional bounding boxes are unsuitable. In lane detection, anchors are often preset starting points and lines with different slopes, with the network predicting the relative distance between the lane and the anchor to optimize shape and position (Chen et al., 2019; Zheng et al., 2022; Ran et al., 2023; Wang et al., 2025). These innovations improve accuracy and efficiency in complex or occluded scenarios.

Research on downstream tasks in adverse weather conditions, such as fog, is limited compared to other detection and segmentation tasks. Traditional solutions often use image enhancement techniques, like dehazing, to improve visual clarity, but this doesn’t always lead to better detection results. Some methods combine image enhancement with detection to reduce weather

interference (Huang et al., 2020), while others simulate foggy images to augment datasets. For example, Nie et al. (Nie et al., 2022) generated foggy images from clear lane images in the CULane dataset, achieving synthetic data augmentation that improved recognition rates from 76.65% to 86.65% under light fog.

Domain adaptation techniques also address the style gap between foggy and clear-weather images (Chen et al., 2018; Zhang et al., 2021). Hnewa et al. (Hnewa and Radha, 2021) proposed a multi-scale domain-adaptive YOLO model, while Li et al. (Li et al., 2023) introduced a transfer learning framework for fog-adaptive object detection using labeled clear-weather and unlabeled foggy images, avoiding the need for annotated foggy datasets.

Traditional dehazing methods suffer from artifacts, whereas deep learning methods using CNNs capture more complex features but require high computational resources and diverse training datasets. However, obtaining real paired images under foggy conditions is challenging, and synthetic images often lead to reduced performance in real-world scenarios.

Lane detection enables key functionalities such as lane departure warnings and autonomous navigation in ADAS. While existing lane detection algorithms perform well under clear weather conditions with visible lane markings, their performance drops significantly in adverse environments like fog, where reduced visibility and image degradation obscure lane clarity, thus increasing the risk of traffic accidents. Furthermore, the lack of specialized datasets tailored to foggy conditions has limited the development of effective deep learning-based solutions for these challenging scenarios.

To address these limitations, we introduce the FoggyLane dataset, a new benchmark specifically designed for lane detection under foggy conditions. This dataset, comprising 1,423 annotated images across six distinct foggy road scenarios, fills a crucial gap in the current lane detection datasets. Additionally, we create foggy versions of two commonly used lane detection datasets, CULane (Pan et al., 2018) and Tusimple (Tusimple, 2017), resulting in the FoggyCULane and FoggyTusimple datasets. These datasets are essential for training and testing lane detection algorithms in foggy environments.

In response to the unique challenges posed by foggy conditions, we propose a robust real-time lane detection method optimized for such environments. The main contributions of our work are as follows:

- 1) To address the issue of missing global information in foggy images, we design a Global Feature Fu-

sion Module (GFFM) within the backbone network to capture relationships between inputs, improving feature extraction in foggy scenarios.

- 2) To enhance the utilization of structural relationships between lane instances, we introduce a Kernel Feature Fusion Module (KFFM) that learns and predicts the correlations between lane instances, improving lane detection accuracy and robustness.
- 3) To tackle the loss of edge information in foggy images, we incorporate a Low-level Edge Enhancement Module (LEEM) that enhances the model’s attention to edge features, improving the accuracy and stability of lane detection.
- 4) To address the lack of open-source foggy lane detection datasets, we construct FoggyLane, a real-world dataset with 1,423 annotated images, and generate FoggyCULane and FoggyTusimple based on existing datasets. Our method achieves state-of-the-art performance with inference speeds of 192.9 FPS on NVIDIA RTX 3090 and 38.4 FPS on NVIDIA Jetson AGX Orin, confirming its real-time capability and practical applicability in real-world settings.

2. Related Work

In recent years, advances in deep learning have substantially improved lane detection performance. Building on these advances, current lane detection methods are divided into four main paradigms: segmentation-based, anchor-based, curve-based, and row-wise-based approaches, according to their modeling strategies.

2.1. Segmentation-based Lane Detection

Segmentation-based methods mainly utilize semantic segmentation or instance segmentation techniques to distinguish lane lines from other objects or backgrounds in the image, transforming lane detection into a pixel-level classification problem. LaneNet(Neven et al., 2018) employs a two-branch structure of split branches and embedded branches, the split branches output a binary lane mask to recognize lane lines, and the embedded branches assign a unique embedding to each pixel to realize the distinction of lane lines. SCNN(Pan et al., 2018) modifies the conventional layer-wise convolution approach by incorporating a slice-wise convolution technique, enabling horizontal and vertical information flow between pixels within a layer. RESA(Zheng et al., 2021) introduces a spatial attention module that ensures robust lane prediction by cyclically shifting the

feature map horizontally and vertically so that each pixel can acquire global information. Although these segmentation-based methods possess high accuracy and robustness, the models are bulky and slow to process due to high consumption of computational resources. HW-Transformer(Zhao et al., 2024) presents an innovative lane detection network to expand the visual range around the lane and enable global information communication through intersecting features, alongside a self-attention knowledge distillation (SAKD) method to enhance performance and semantic feature learning.

2.2. Curve-based Lane Detection

Curve-based methods transform the lane detection into a regression task by predicting polynomial coefficients that fit lane lines to polynomial equations. PolyLaneNet(Tabelini et al., 2021b) proposes an end-to-end convolutional neural network that transforms images into polynomials representing each lane’s markers, along with domain-specific lane polynomials and confidence values for every lane. Similarly, LSTR(Liu et al., 2021b) utilizes a Transformer-based architecture that captures both local lane structures and broader contextual information through non-local interactions. DB-Net(Dai et al., 2024) introduces NURBS curves and utilizes their geometric semantic properties to achieve local and global optimization, which improves the robustness of lane line detection and model interpretation. However, polynomial fitting is sensitive to parameter selection, and minor changes in parameters can result in significant variations in fitting results, leading to unstable lane line detection.

2.3. Anchor-based Lane Detection

Anchor-based approaches employ predetermined reference lines within the image space to generate lane predictions, subsequently calculating necessary offsets to precisely match these anchors with true lane markings. Line-CNN(Li et al., 2019) introduces the anchor mechanism into lane detection for the first time, and innovatively proposes line anchors. LaneATT(Tabelini et al., 2021a) effectively solves the problem of occlusion and illumination due to the lack of a line anchor, by fusing extracted anchor features with global features generated by attention module. CLRNet(Zheng et al., 2022) employs a coarse-to-fine detection strategy, where lane lines are first approximated using high-level semantic cues before being refined with detailed low-level features. This hierarchical fusion of semantic information significantly improves detection precision. FLAM-Net(Ran et al., 2023) employs an adaptive line anchor

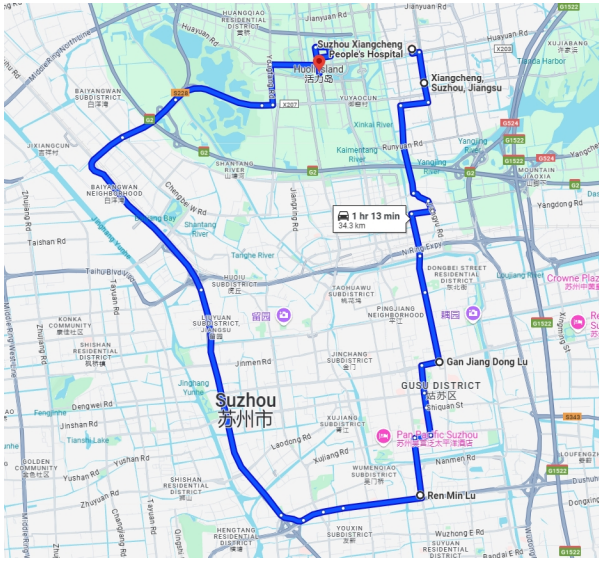


Figure 2: The route for dataset acquisition in Suzhou on the morning of October 26, 2023.(GoogleMaps, Accessed: 2024)

strategy, augmented by patch-based feature pooling and decomposed self-attention mechanisms. This design strengthens both local feature extraction and global context modeling, improving performance in handling intricate lane structures. However, due to the multiple curvature and orientation variations of lane lines in the real world, the performance of the anchor-based methods may be limited in capturing precise paths with complex shapes.

2.4. Row-wise-based Lane Detection

Row-wise methods predict lane positions for each image row. E2E-LMD(Yoo et al., 2020) introduces the row-wise-based lane detection task and develops a complete architecture that outputs lane marker positions directly. UFLD(Qin et al., 2020) utilizes global features to select the lane positions of predefined rows of an image and proposes a structural loss function, so as to ensure the continuity and smoothness of the lanes. Cond-LaneNet(Liu et al., 2021a) utilizes conditional convolution and row-by-row prediction strategies to enhance lane recognition accuracy, and introduces the RIM module to effectively address complex lane layouts. The row-wise-based detection methods improve computational efficiency by focusing only on the row regions in the image, and possesses high detection accuracy while maintaining efficiency.

3. Data Constrution

Due to the data-driven nature of deep learning models, the quality, size, and diversity of the datasets largely determine the applicability and performance of such models. In the task of lane detection, models trained solely on clear weather data struggle to adapt to low-visibility foggy conditions. Issues such as blurred lane boundaries, faded lane colors, and reduced image quality often arise in fog, making lane detection more challenging. Therefore, training with a foggy weather lane dataset can significantly improve an autonomous driving system’s ability to handle such conditions, enhancing both detection accuracy and overall reliabil-

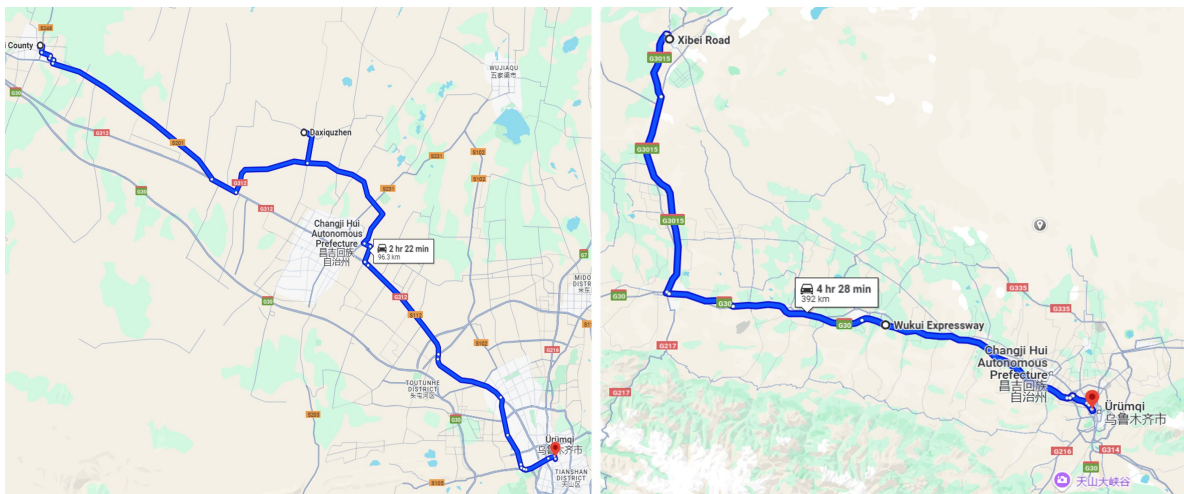


Figure 3: The routes for dataset acquisition in Urumqi, Xinjiang Autonomous Region: the left illustrates the morning of December 9, 2023, while the right depicts the evening of January 2, 2024.(GoogleMaps, Accessed: 2024)

Table 1: Comparison Between Our Dataset and Existing Lane Detection Datasets

Dataset	Frames	Multi-traffic scenarios	Instance-level annotation	Number of foggy datasets	Resolution
Caltech-Lanes (Aly, 2008)	1.2k	✗	✓	None	640 x 480
Tusimple (Tusimple, 2017)	6.4k	✗	✓	None	1280 x 720
LLAMAS (Behrendt and Soussan, 2019)	100k	✓	✓	None	1276 x 717
Appolloscape (Huang et al., 2018)	110k	✓	✗	None	3384 x 2710
BDD100k (Yu et al., 2020)	100k	✓	✗	None	1280 x 720
CULane (Pan et al., 2018)	133k	✓	✓	None	1640 x 590
CurveLanes (Xu et al., 2020)	150k	✓	✓	None	1280 x 720
FoggyLane (ours)	1.423k	✓	✓	1.5k	1640 x 590

ity. However, there is currently no publicly available foggy weather lane detection dataset. To fill this gap, we created the FoggyLane dataset for lane detection in foggy weather. In addition, we generated two supplementary datasets, FoggyCULane and FoggyTusimple, by using fog modeling techniques on existing CULane (Pan et al., 2018) and Tusimple (Tusimple, 2017) datasets to test the generalizability of our methods.

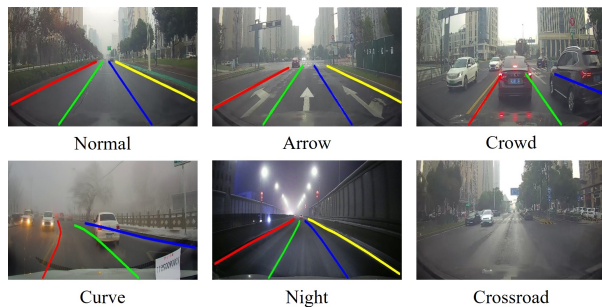


Figure 4: The different road types of FoggyLane images examples.

3.1. FoggyLane

Existing lane detection algorithms for intelligent connected vehicle ADAS systems perform well under favorable weather conditions, but their performance significantly deteriorates in adverse conditions like fog, which reduces visibility and increases the likelihood of traffic accidents. Current benchmark datasets, including CULane (Pan et al., 2018), Tusimple (Tusimple, 2017), and LLAMAS (Behrendt and Soussan, 2019), lack foggy weather data. To address this, we developed FoggyLane, a dataset specifically designed for foggy conditions. Data was collected using a monocular forward-facing camera at various times and locations, including Suzhou and Urumqi, China, between October 2023 and January 2024. The dataset includes 1,086 images at various resolutions, which were resized to 1640×590 for consistency.

Since foggy conditions are rare, we extended the dataset by incorporating foggy driving scenes from two

YouTube videos (YouTube, Accessed: 2024), resulting in an additional 337 images. The final FoggyLane dataset contains 1,423 images, covering six road scenes: Normal, Arrow, Crowd, Curve, Night, and Crossroad. The dataset was partitioned into training, validation and testing sets, with stratification to maintain a consistent distribution of scene types across both subsets.

Comparing FoggyLane with existing datasets, such as Caltech-Lanes (Aly, 2008) and Tusimple (Tusimple, 2017), which focus on single traffic scenarios, and LLAMAS (Behrendt and Soussan, 2019), which uses high-precision map annotations, we found that these datasets do not cover foggy weather scenarios. While ApolloScape (Huang et al., 2018) and BDD100k (Yu et al., 2020) include multiple traffic scenarios, they lack instance-level annotations. Similarly, although CULane (Pan et al., 2018) and CurveLanes (Xu et al., 2020) cover a wide range of traffic scenes, they do not include foggy conditions. Models trained on datasets limited to clear weather struggle in fog, where lane boundaries are blurred and image quality reduced. To fill this gap, FoggyLane offers a thorough solution for lane detection in foggy conditions with instance-level annotations.

Our dataset has two key advantages:

Pioneering foggy lane detection dataset: FoggyLane is a dataset specifically designed to address foggy weather scenarios. It covers a range of challenging conditions, including foggy congested roads, foggy curves, and foggy night roads. This dataset is crucial for testing the robustness of ADAS under adverse conditions.

Strict annotation standards: The dataset follows strict annotation guidelines, including marking the center of lanes, connecting lane markings at intersections, and prioritizing solid lines over grid lines, etc. (Zhang et al., 2024a). These rigorous annotations can significantly improve the accuracy and consistency of lane detection in foggy weather, thus enhancing the stability and safety of autonomous driving systems and providing

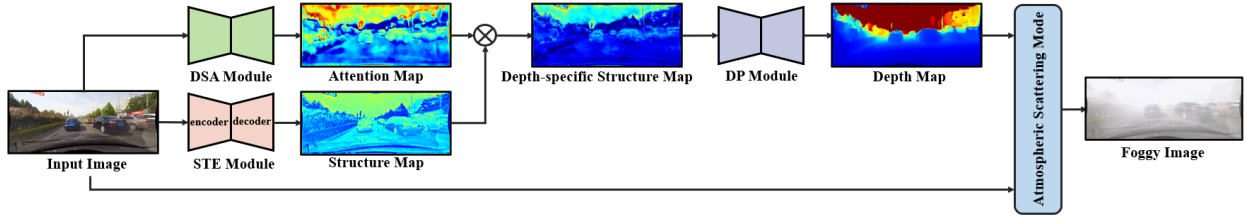


Figure 5: Networks of foggy image generation. \otimes represents element-wise multiplication.

a solid data foundation for the reliable deployment of autonomous technology.

3.2. FoggyCULane and FoggyTuSimple

Currently, numerous datasets are available for lane detection. Among them, we select two widely adopted and representative benchmarks: CULane(Pan et al., 2018) and TuSimple(Tusimple, 2017). The CULane dataset (Pan et al., 2018) serves as an extensive and demanding benchmark, encompassing various scenarios such as highways, urban roads, and rural regions in Beijing. In contrast, the TuSimple dataset (Tusimple, 2017) primarily comprises daytime driving videos collected on American highways, featuring a variety of lighting

conditions and complex traffic situations. Based on these datasets, we generate synthetic foggy versions, named FoggyCULane and FoggyTuSimple, to facilitate evaluation under adverse weather conditions.

The method for generating foggy images is inspired by the model (Nie et al., 2022), and the complete generation process is shown in Fig. 5. To be specific, the atmospheric scattering model can effectively utilize prior information to analyze the degradation mechanisms of image quality in foggy conditions. It models foggy images as a combination of scattered light and direct light based on optical principles, ultimately synthesizing a clear image into a foggy one. The mathematical modeling equation defined by Koschmieder (Harald, 1924) is

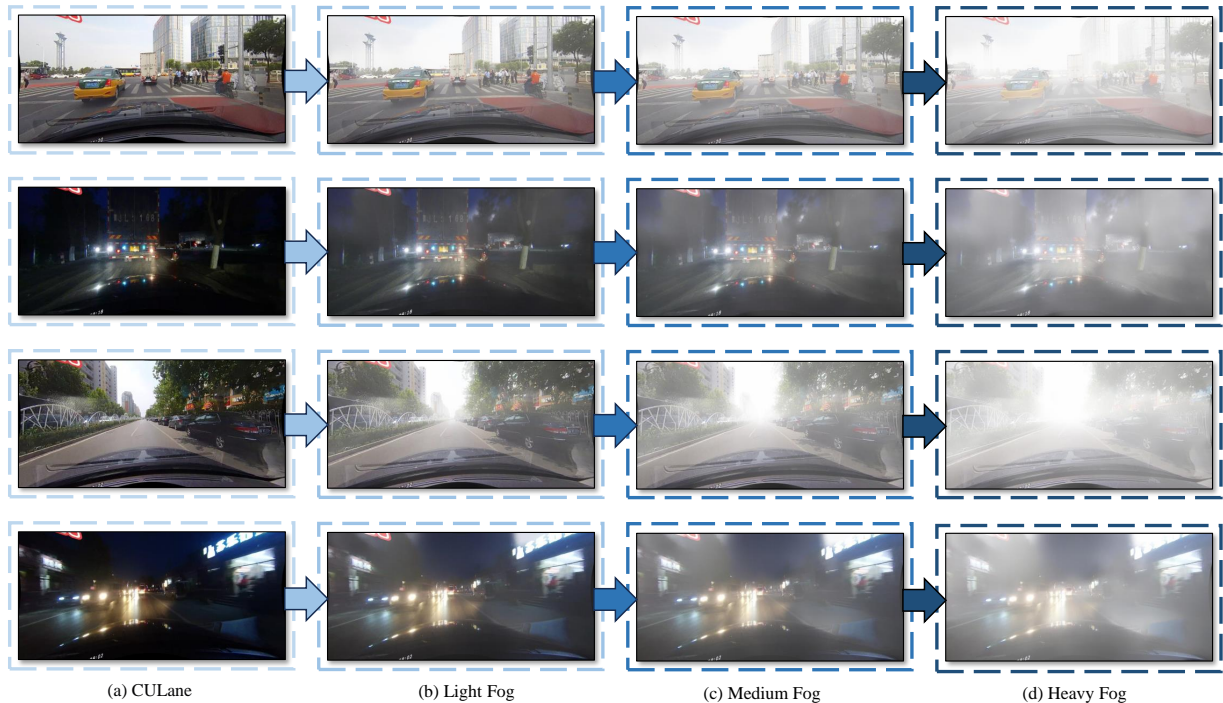


Figure 6: The FoggyCULane dataset examples. (a) is the original CULane dataset. And (b) to (d) are the foggy images of different concentrations with β values of 2, 4, and 8, respectively.

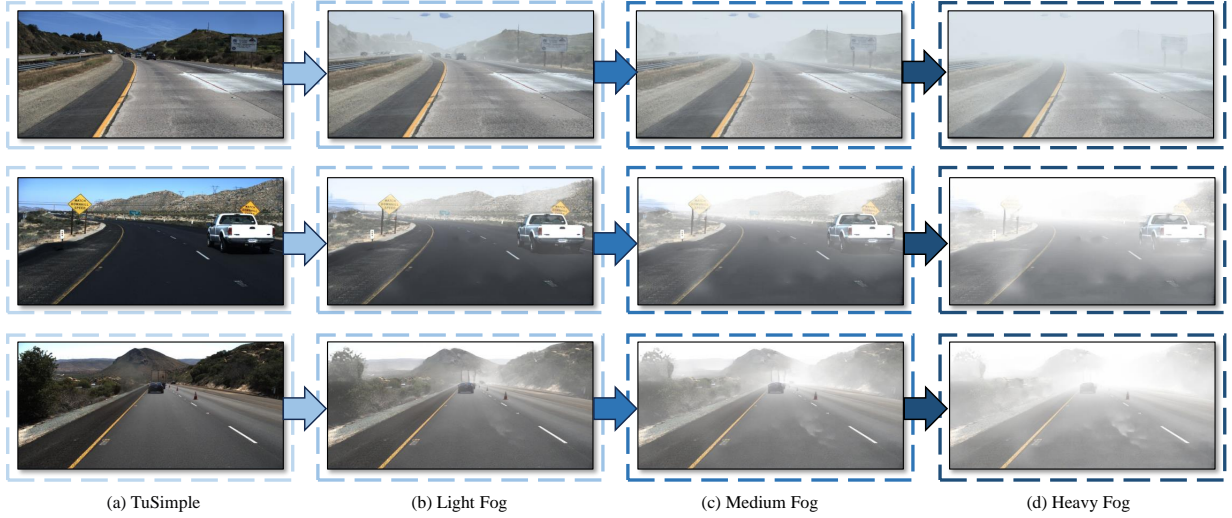


Figure 7: The FoggyTuSimple dataset examples. (a) is the original TuSimple dataset. And (b) to (d) are the foggy images of different concentrations with β values of 2, 4, and 8, respectively.

represented as:

$$I(x) = J(x)t(x) + A(1 - t(x)) \quad (1)$$

where x indicates a certain pixel of the image, $J(x)$ refers to the original clear image of the object and $I(x)$ refers to the foggy image. A is the atmospheric light value at infinity and $t(x)$ can be further defined as:

$$t(x) = e^{-\beta d(x)} \quad (2)$$

where β is the extinction coefficient, which is closely related to the concentration, size, type and distribution of particulate matter. $d(x)$ represents the distance between the object and the viewer. As this distance increases, the transmittance decreases, resulting in thicker fog.

To calculate the corresponding $d(x)$, we use the S2R-DepthNet(Chen et al., 2021) that has good generalization performance across various applications. The S2R-DepthNet consists of three modules that decouple the structural and textural information of the input image. Then they suppress information irrelevant to depth and use structural information for depth prediction. The Structure Extraction Module (STE) breaks down the image to capture domain-independent structural details. The Depth-specific Attention (DSA) generates an attention map from the original image. Once processed through the DSA and STE Modules, as depicted in Fig. 5, the attention map and structural map are multiplied to produce a refined and all-encompassing depth-specific structure map. The Depth Prediction (DP) module is then responsible for estimating the depth.

According to the transmittance formula Eq. (2), we use the dark channel prior(He et al., 2011) to calculate the average atmospheric light value A . In the non-sky area of an outdoor clear image, there is usually at least one very small or close to zero value in the RGB image for each pixel, which is called the dark channel of that pixel. Therefore, for any image I , the mathematical formula for its corresponding dark channel image $I_{\text{dark}}(x)$ can be defined as:

$$I_{\text{dark}}(x) = \min_{c \in R, G, B} \left(\min_{y \in \Omega(x)} I_c(y) \right) \quad (3)$$

where $I_c(y)$ is the value of the c -th channel of image I at pixel point y , and $\omega(x)$ is a small region around pixel point x . In the dark channel, find the top 0.1% brightest pixels and take the maximum value of their RGB channels as an approximation of the average atmospheric light value A . After obtaining the transmittance and the average atmospheric light value, the images of light fog, medium fog, and heavy fog can be obtained by fine-tuning the extinction coefficient β . The original images and the foggy images generated under different β values are displayed in Figs. 6 and 7.

4. Methods

4.1. Overall structure

To address the challenge of lane detection in foggy conditions, where visibility is significantly reduced, we propose a fog-enhanced lane detection network inspired by row-wise methods. As illustrated in the Fig. 8, the

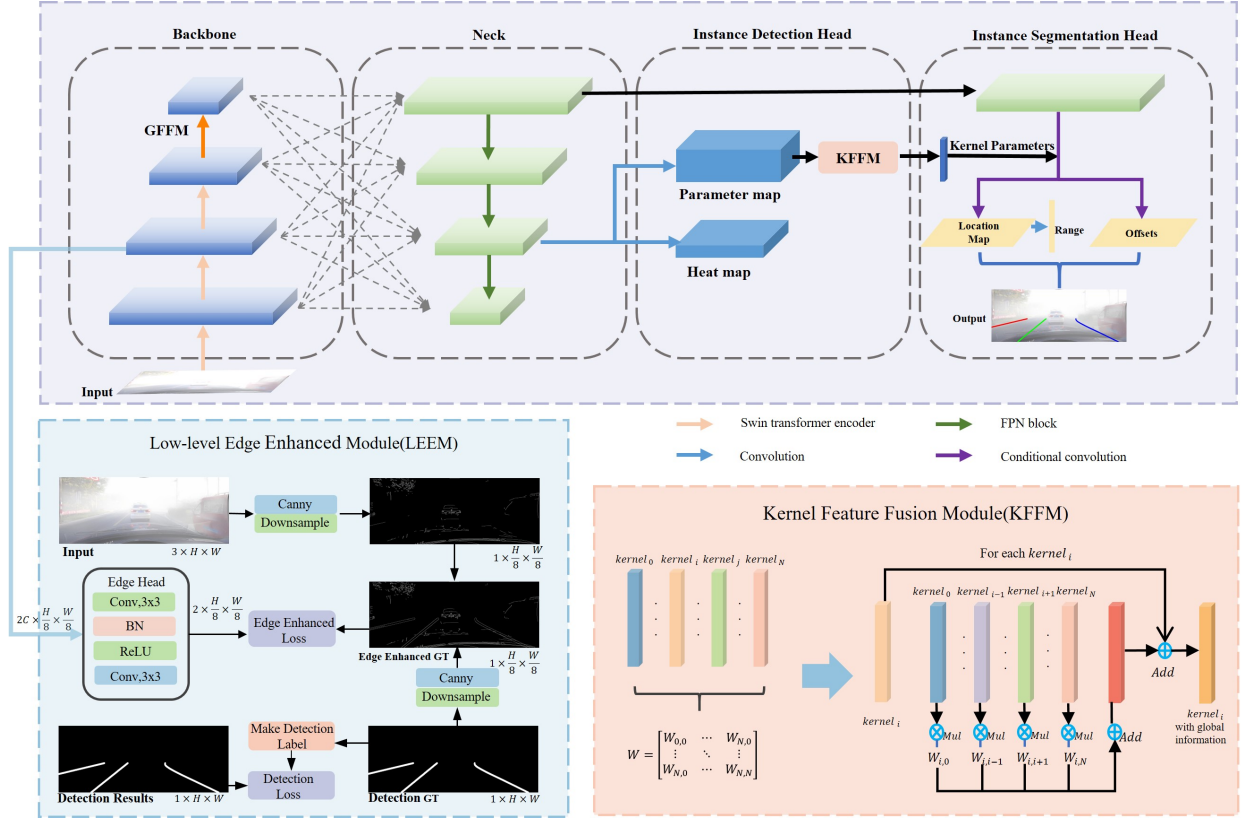


Figure 8: Overview of the proposed network.

network comprises four main components. To mitigate the loss of global information in foggy images, we introduce a global feature fusion module within the backbone network. In the neck network, we utilize HR-NetV2(Wang et al., 2021) to further integrate multi-scale features from different stages of the backbone, enabling the aggregation of information across various scales and resolutions.

For the detection head, we employ the concept of dynamic convolution, incorporating both lane instance detection and lane mask segmentation. During instance detection, the network identifies lane instances within the image and predicts a set of dynamic convolution kernel parameters for each lane. These parameters are subsequently applied to the lane mask segmentation head to filter the instance-specific segmentation map for each lane. This approach eliminates the need for complex post-processing steps, enhancing detection speed.

Moreover, to fully exploit the structural relationships between lane lines, we designed a kernel feature fusion module, which allows the network to automatically learn the correlations between predicted lane instances. This contributes to more accurate lane identification and

localization. Additionally, to compensate for the loss of edge information in foggy images, we incorporated a low-level edge enhancement module, further improving the network’s ability to detect lane boundaries with precision.

4.2. Global Feature Fusion Module

In recent years, Transformer architectures have made considerable strides in the field of natural language processing, leading researchers to explore their applications in computer vision. With self-attention mechanisms, Transformer models can capture dependencies between different regions and pixels within an image, thus facilitating a better understanding of global image information. As a result, Transformer models have demonstrated outstanding modeling capabilities and performance improvements in various traffic vision tasks(Zhang et al., 2025; Chen et al., 2023). However, applying Transformers to the visual domain still faces some challenges. Firstly, traditional Transformer architectures lack the hierarchical structure and down-sampling operations found in CNN models, making

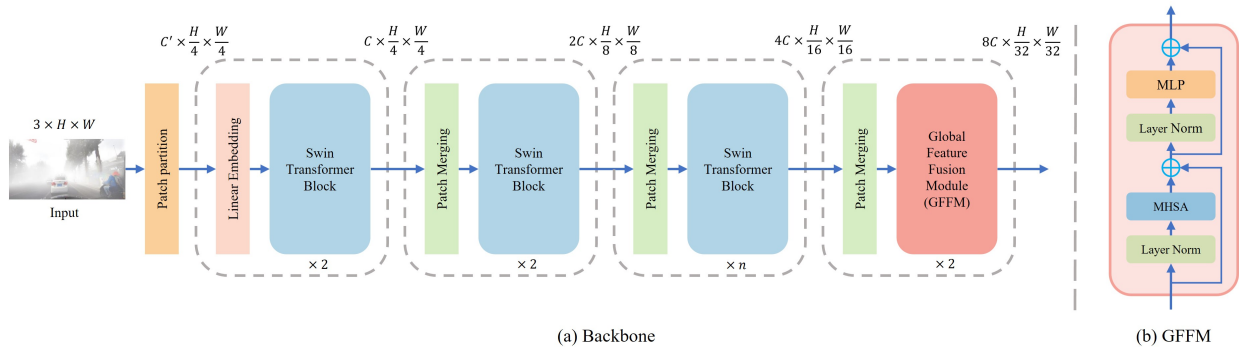


Figure 9: Backbone Network with Global Feature Fusion.

them less adaptable to changes in resolution and receptive field, which may hinder handling of complex visual entities. Additionally, calculating global attention at high resolutions can be computationally intensive.

To address these issues, researchers have proposed several enhanced architectures, such as hierarchical Transformers (Liu et al., 2021c, 2022; Dong et al., 2022). Among them, the Swin Transformer (Liu et al., 2021c) combines CNN-inspired concepts, integrating local perception with global attention in a hierarchical Transformer framework. As the Swin Transformer has shown strong performance in classification, detection, and segmentation tasks, balancing computational efficiency with accuracy, we chose the Swin Transformer as our backbone network. However, since the Swin Transformer’s window attention mechanism primarily focuses on local features, its hierarchical structure may still lack sufficient global context for foggy scene understanding. Therefore, as illustrated in the Fig. 9, we designed a Global Feature Fusion Module (GFFM) to enhance the network’s global information integration. Specifically, we replaced the window attention mechanism in the final stage with a standard multi-head attention mechanism to capture global correlations across all inputs. At this stage, image resolution has been sufficiently reduced, making the computational cost of global attention manageable.

4.3. Kernel Feature Fusion Module

Dynamic convolution adjusts convolutional kernel parameters based on input data, enhancing network flexibility and generalization compared to traditional convolution. CondInst (Tian et al., 2023) is an instance segmentation framework using dynamic convolution to generate kernel parameters for each instance, reducing network load and improving efficiency. Similarly,

CondLane (Liu et al., 2021a) applies dynamic convolution for lane instance segmentation, achieving strong performance.

Building on this, our lane detection head also uses dynamic convolution, consisting of lane instance detection and mask segmentation. Unlike traditional methods, we generate dynamic convolution kernels using the lane’s starting position features rather than center features, which are more suitable for the elongated nature of lanes. We design an instance detection head with two branches: one predicts lane starting points and generates a heatmap, and the other generates dynamic convolution kernels for lane segmentation.

However, existing methods don’t fully utilize the structural relationships between lane instances. To address this, we introduce a Kernel Feature Fusion Module (KFFM) that enables the network to learn and predict relationships between lane instances, enhancing detection performance. KFFM is shown in the bottom right of Fig. 8.

4.4. Low-level Edge Enhanced Module

Images in foggy conditions differ from those captured under good lighting primarily due to their blurriness and low contrast. This effect renders the edges of objects and details within the scene indistinct and hard to detect, impacting the algorithm’s ability to understand and recognize the scene accurately. Edge information, beyond simply marking object boundaries, also implicitly contains structural and spatial information about objects, forming a critical foundation for tasks such as object detection, segmentation, and tracking. Using the Canny edge detection algorithm with identical threshold settings, we processed both foggy and normal images, as shown in the Fig. 10. It is evident that fog significantly degrades edge information, particularly affecting lane line edges, which become nearly

indiscernible. Given that lane detection relies heavily on edge information—lane positioning is typically determined by the boundary between lane edges and the road background—both global scene information and detailed edge information are essential for accurate lane detection. To address the challenges of lane detection in

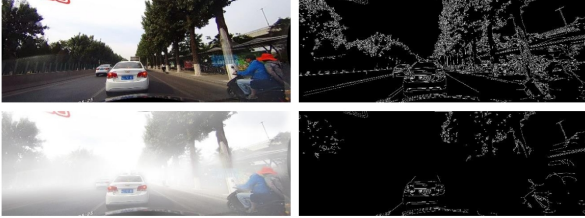


Figure 10: Comparison of edge information between foggy and normal scenarios.

foggy conditions, we apply global feature fusion within both the backbone network and detection head to enhance high-dimensional global features. Additionally, we use multi-scale fusion to aggregate detail features from low-resolution feature maps. However, this approach alone does not fully compensate for the loss of edge detail inherent in foggy images. Therefore, we introduce a Low-level Edge Enhanced Module (LEEM) into the network to boost the network’s focus on edge information, thereby improving both the accuracy and stability of lane detection.

Specifically, we add an auxiliary path in the network to learn the edge features of the input image. First, we apply the Canny operator to the input image for edge detection, supplemented by lane line labels to reconstruct any missing lane edges, generating the training labels for the edge enhancement module. To avoid interfering with high-level semantic extraction and subsequent detection segmentation, while strengthening the low-level network’s learning of edge textures and other low-dimensional features, we introduce a branch at the second stage of the backbone network. This branch sequentially applies a 3×3 and a 1×1 convolution. We then compute the cross-entropy loss between the branch output and the edge labels. The detailed structure is illustrated in the bottom-left of the Fig. 8. Notably, this auxiliary enhancement path is only active during training, thus not increasing computation or processing time during deployment.

4.5. Loss functions

Based on the above, our method involves a total of five prediction tasks: lane start point prediction, row-based segmentation prediction, vertical range predic-

tion, offset prediction, and edge prediction. The loss functions for each task are detailed below.

4.5.1. Lane start point prediction

In feature maps with a large receptive field and low resolution, the lane line start point is difficult to be accurately represented by a single pixel location. Moreover, in such large receptive field feature maps, pixels near the target point exhibit similar features. If these pixels are directly labeled as negative samples, it will interfere with the network training and make it difficult for the network to learn and optimize. Therefore, this method uses a Gaussian kernel function to generate a heatmap label for the lane line start point. Each element in the heatmap label represents the confidence that the position corresponds to the target point; the closer to the target point, the higher the confidence, and the farther away, the lower the confidence. In other words, the ground truth is softly labeled with a Gaussian function, making it easier for the network to converge. Suppose (x, y) denotes a position on the low-resolution feature map, and (p_x, p_y) represents the coordinate of the target point on the low-resolution feature map. Then, the ground truth heatmap GT value at position (x, y) is defined as:

$$GT(x, y) = \exp\left(-\frac{(x - p_x)^2 + (y - p_y)^2}{2\sigma^2}\right) \quad (4)$$

where σ controls the decay rate of the Gaussian kernel. A larger σ results in slower confidence decay and thus a larger heatmap area.

This method combines the Gaussian heatmaps of all lane line start points within the image into a single heatmap. When multiple heatmaps respond at the same location, the maximum value is retained to form the final ground truth heatmap. Then, the Focal Loss is used to calculate the loss between the predicted heatmap and the ground truth heatmap. Let the predicted heatmap value at position (x, y) be P_{xy} , and let N be the total number of pixels in the heatmap. The Focal Loss between the predicted heatmap and the ground truth heatmap is defined as:

$$\mathcal{L}_{hm} = -\frac{1}{N} \sum_{x,y} \begin{cases} (1 - P_{xy})^\alpha \log(P_{xy}), & \text{if } GT(x, y) = 1 \\ (1 - GT(x, y))^\beta (P_{xy})^\alpha \log(1 - P_{xy}), & \text{otherwise} \end{cases} \quad (5)$$

4.5.2. Row-based segmentation prediction

Row-based segmentation predicts a horizontal coordinate $E(\hat{x}_i)$ for each row. For this task, our method

Table 2: Comparison with Advanced Lane Detection on FoggyLane dataset.

Method	Venue	Backbone	F1@50	F1@65	F1@75	F1@85	mF1	Gflops(G)	FPS
SCNN(Pan et al., 2018)	AAAI 2018	VGG16	84.01	62.08	56.34	12.76	41.78	328.4	18.7
UFLD(Qin et al., 2020)	ECCV 2020	ResNet18	81.76	56.54	32.32	6.50	38.24	8.4	327.3
UFLD(Qin et al., 2020)	ECCV 2020	ResNet34	82.75	61.25	34.44	7.89	40.23	16.9	176.9
LaneATT(Tabelini et al., 2021a)	CVPR 2020	ResNet18	81.98	59.61	34.78	7.69	40.06	9.3	247.7
LaneATT(Tabelini et al., 2021a)	CVPR 2020	ResNet34	84.32	63.08	38.91	10.76	42.63	18.0	167.1
LSTR(Liu et al., 2021b)	WACV 2021	ResNet34	83.79	68.23	58.29	25.32	48.91	-	124.4
RESA(Zheng et al., 2021)	AAAI 2021	ResNet34	85.19	65.89	61.89	14.57	48.75	41.0	76.7
RESA(Zheng et al., 2021)	AAAI 2021	ResNet50	86.24	69.22	65.27	16.55	52.34	43.0	53.0
CondLane(Liu et al., 2021a)	ICCV 2021	ResNet18	90.38	75.08	47.50	47.50	10.96	10.2	194.7
CondLane(Liu et al., 2021a)	ICCV 2021	ResNet34	90.58	78.45	56.48	15.59	52.25	19.6	136.5
CLRNet(Zheng et al., 2022)	CVPR 2022	ResNet34	91.56	82.43	65.61	30.20	58.14	21.5	90.0
CLRNet(Zheng et al., 2022)	CVPR 2022	DLA34	92.09	83.98	72.15	41.61	62.28	18.5	81.3
FLAMNet(Ran et al., 2023)	IEEE TITS 2023	ResNet34	89.94	78.90	55.32	12.96	50.99	30.1	32.0
FLAMNet(Ran et al., 2023)	IEEE TITS 2023	DLA34	91.16	82.77	64.95	24.22	56.70	21.7	31.7
DBNet(Dai et al., 2024)	IEEE TIV 2024	ResNet18	89.61	81.27	65.27	26.15	56.52	22.6	147.6
DBNet(Dai et al., 2024)	IEEE TIV 2024	ResNet34	90.02	83.44	71.66	40.51	60.94	32.1	129.0
HWLane(Zhao et al., 2024)	IEEE TITS 2024	Res34	91.99	84.23	68.08	35.27	34.38	18.6	70.0
PolarRCNN(Wang et al., 2025)	IEEE TITS 2025	ResNet34	91.07	79.38	57.44	14.74	52.42	19.0	171.6
PolarRCNN(Wang et al., 2025)	IEEE TITS 2025	DLA34	90.02	83.44	71.66	40.51	51.97	16.0	150.4
Ours	-	SwinGFFM-t	92.34	84.65	70.99	35.77	60.82	12.0	70.4 / 304.7*
Ours	-	SwinGFFM-s	95.04(2.95↑)	88.61(4.63↑)	77.32(5.17↑)	45.02(3.41↑)	65.60(3.32↑)	20.3	38.2 / 192.9*

Note: For a fairer comparison, we re-evaluated the FPS of the source code available detectors using one NVIDIA GeForce RTX 3090 GPU on the same machine. * indicates the FPS after acceleration with TensorRT.

uses the L1 loss function to optimize the predicted coordinates. Suppose V denotes the effective vertical range of the lane line, N_v is the number of effective rows, and x_i is the ground truth horizontal coordinate. The loss function is defined as:

$$L_{\text{row}} = \frac{1}{N_v} \sum_{i \in V} |E(\hat{x}_i) - x_i| \quad (6)$$

4.5.3. Vertical range prediction

For the label of the lane line vertical range vector prediction, our method uses a $1 \times Y$ vector representation. If the lane line passes through the Y_i row, its value is 1; otherwise, it is 0. Thus, this can be regarded as a segmentation task. Our method optimizes it using the cross-entropy loss function. Suppose v_i denotes the predicted probability that the i -th row is positive, then the loss function is defined as:

$$L_{\text{range}} = \sum (-y_{gt}^i \log(v_i) - (1 - y_{gt}^i) \log(1 - v_i)) \quad (7)$$

4.5.4. Offset prediction

Firstly, the generation of ground truth labels for offset prediction is required. For each lane line, the proposed method constructs the ground truth offset as the horizontal displacement relative to the lane centerline for each grid cell within a specified width. The predicted offsets are optimized using an L1 loss function. Let δ_{xy} denote the ground truth offset at coordinate (x, y) , $\hat{\delta}_{xy}$ the predicted offset, and Ω the region surrounding the lane line. The loss function is then formulated as follows:

$$L_{\text{offset}} = \frac{1}{N_{\Omega}} \sum_{(x,y) \in \Omega} |\hat{\delta}_{xy} - \delta_{xy}| \quad (8)$$

4.5.5. Edge prediction

For the task of edge enhancement, the method treats it as an edge segmentation problem, which is essentially a binary classification task. The labels at edge locations are assigned a value of 1, while non-edge locations are assigned 0. Accordingly, the cross-entropy loss function is employed for optimization. Let e_{gt}^i denote the label of pixel i , and p_i represent the predicted probability of the pixel being positive. The loss function is defined as:

$$L_{\text{edge}} = \sum_i (-e_{gt}^i \log(p_i) - (1 - e_{gt}^i) \log(1 - p_i)) \quad (9)$$

4.5.6. Total loss

To balance the influence of different tasks on the overall training of the network, a weighted fusion of the loss functions for each sub-task is employed. The total loss function is formulated as follows:

$$L_{\text{total}} = \alpha L_{hm} + \beta L_{\text{row}} + \gamma L_{\text{range}} + \delta L_{\text{offset}} + \varepsilon L_{\text{edge}} \quad (10)$$

where the network achieves optimal performance when the weights are set as $\alpha = 1$, $\beta = 1$, $\gamma = 1$, $\delta = 0.4$, and $\varepsilon = 0.1$.

5. Experiments

5.1. Datasets

In the Data Construction chapter, we introduce the FoggyLane dataset, which was constructed from real-world collections for foggy lane detection, along with the FoggyCULane and FoggyTusimple datasets that



Figure 11: Visualization results of CLRNet(Zheng et al., 2022), FLAMNet(Ran et al., 2023), PolarRCNN(Wang et al., 2025) and our method on FoggyLane testing set. The arrows indicate instances of lane lines that were not correctly detected by the corresponding method.

were synthesized through modeling foggy images. Our method is evaluated on these three datasets.

FoggyLane is a lane detection dataset specifically designed for foggy scenarios, containing 1,423 frames of foggy lane images for training and testing. All images are of resolution 1640x590 pixels.

FoggyCULane is synthesized from the large-scale challenging lane detection dataset CULane using a foggy image modeling approach. It maintains the same number of images as CULane. The resolution of all images is also 1640x590 pixels.

FoggyTusimple is synthesized from Tusimple through the foggy image modeling method. At the same time, the dataset follows the same structure as Tusimple, comprising 3,268 training images, 358 validation samples, and 2,782 test cases. All visual data maintains a consistent resolution of 1280x720 pixels.

5.2. Evaluation Metric

Lane detection is typically approached as a semantic segmentation problem, assessed using common metrics. However, due to its distinct characteristics, lane detection also requires specialized evaluation metrics. Adhering to SCNN’s (Pan et al., 2018) framework, we link labeled or predicted lane points to form line segments and extend them into 30-pixel-wide regions. Subsequently, we compute the Intersection over Union (IoU), and if the IoU value exceeds a predefined threshold, typically set at 0.5, the prediction is considered correct. From

this, we calculate Precision, Recall, and F1-score using the following formulas:

$$F1 = \frac{2 \times Precision \times Recall}{Precision + Recall} \quad (11)$$

$$Precision = \frac{TP}{TP + FP} \quad (12)$$

$$Recall = \frac{TP}{TP + FN} \quad (13)$$

For the FoggyTusimple dataset, we use the same evaluation metrics as the Tusimple dataset. The official Tusimple dataset includes three standard metrics: false positive rate (FPR), false negative rate (FNR), and accuracy. The formula for calculating accuracy is as follows:

$$Accuracy = \frac{\sum_{clip} C_{clip}}{\sum_{clip} S_{clip}} \quad (14)$$

where C_{clip} represents the number of correctly predicted lane points in the image, while S_{clip} denotes the total number of ground truth lane points.

5.3. Implementation Details

We conducted experiments on the NVIDIA GeForce RTX 3090 platform. The SwinGFFM backbone network was pre-trained on the COCO dataset for 500

Table 3: Comparison with Advanced Lane Detection on FoggyCULane dataset

Method	Venue	Backbone	Normal	Crowded	Dazzle light	Shadow	No line	Arrow	Curve	Cross	Night	Total
SCNN(Pan et al., 2018)	AAAI 2018	VGG16	91.07	71.32	67.23	65.23	49.14	88.06	67.07	1344	70.78	72.94
UFLD(Qin et al., 2020)	ECCV 2020	ResNet18	87.57	65.47	55.21	60.38	38.66	82.26	57.29	1849	60.61	67.69
UFLD(Qin et al., 2020)	ECCV 2020	ResNet34	89.10	68.29	60.91	62.03	41.98	85.17	63.88	2371	70.13	70.13
LaneATT(Tabelini et al., 2021a)	CVPR 2020	ResNet18	90.52	71.52	65.70	68.92	47.31	86.32	62.34	870	67.64	74.30
LaneATT(Tabelini et al., 2021a)	CVPR 2020	ResNet34	91.68	72.93	67.23	65.23	49.14	88.06	67.07	1344	70.78	75.53
LSTR(Liu et al., 2021b)	WACV 2021	ResNet34	85.79	63.45	56.73	58.72	38.20	79.31	55.34	1068	57.62	65.64
RESA(Zheng et al., 2021)	AAAI 2021	ResNet34	90.97	72.32	67.31	74.01	46.52	86.32	65.26	1536	73.62	74.97
RESA(Zheng et al., 2021)	AAAI 2021	ResNet50	92.09	73.49	67.40	73.87	47.92	87.48	69.28	1722	69.85	75.19
CondLane(Liu et al., 2021a)	JCCV 2021	ResNet18	91.56	74.41	71.12	77.89	48.59	86.73	71.34	1262	71.00	76.46
CondLane(Liu et al., 2021a)	JCCV 2021	ResNet34	91.76	75.55	69.62	74.62	50.01	87.40	71.29	1427	72.11	77.06
CLRNet(Zheng et al., 2022)	CVPR 2022	ResNet34	92.96	76.32	73.40	79.06	51.46	89.39	71.83	1301	73.64	78.36
CLRNet(Zheng et al., 2022)	CVPR 2022	DLA34	93.23	77.64	73.90	79.23	52.11	89.45	72.48	1109	73.63	79.04
FLAMNet(Ran et al., 2023)	IEEE TITS 2023	ResNet34	92.60	76.61	71.42	79.81	50.89	89.04	71.47	1073	74.17	78.45
FLAMNet(Ran et al., 2023)	IEEE TITS 2023	DLA34	92.98	77.26	71.84	79.76	51.29	89.34	71.38	1143	73.93	78.77
DBNet(Dai et al., 2024)	IEEE TIV 2024	ResNet18	84.91	69.27	60.86	67.94	45.69	79.04	67.50	1045	68.57	71.33
DBNet(Dai et al., 2024)	IEEE TIV 2024	ResNet34	85.61	69.35	61.22	66.50	45.73	79.19	66.51	837	69.93	71.87
HWLane(Zhao et al., 2024)	IEEE TITS 2024	Res34	90.85	73.32	67.18	75.32	47.18	87.14	63.38	1456	69.20	74.61
PolarRCNN(Wang et al., 2025)	IEEE TITS 2025	ResNet34	93.34	77.76	75.26	79.76	53.25	89.62	75.94	1289	74.54	78.68
PolarRCNN(Wang et al., 2025)	IEEE TITS 2025	DLA34	92.90	77.50	74.03	80.89	51.71	89.76	73.02	1226	74.21	79.13
Ours	-	SwinGFFM-t	92.68	77.50	71.52	80.42	50.95	88.92	72.08	950	73.11	78.66
Ours	-	SwinGFFM-s	93.40(0.07)	78.63(0.87)	73.89	82.74(1.85)	53.75(0.50)	89.82(0.37)	74.09	1146	74.97(0.76)	79.85(0.72)

Note: Our method attains state-of-the-art (SOTA) results in multiple scenarios including Normal, Crowded, Shadow, No-line, Arrow and Night conditions, as well as in the overall (Total) performance.

epochs. During lane detection training, we loaded the pre-trained weights and resized input images to 800×320 . Various data augmentation techniques, including rotation, flipping, brightness adjustment, and random scaling, were applied. For full network parameters and training details, please refer to our open-source code.

To benchmark against existing methods(Pan et al., 2018; Zheng et al., 2021; Tabelini et al., 2021a; Zheng et al., 2022; Ran et al., 2023; Liu et al., 2021b; Dai et al., 2024; Qin et al., 2020; Liu et al., 2021a; Wang et al., 2025), we followed the training settings provided in the respective papers. For FoggyCULane and FoggyTusimple, we adopted the training parameters from the original CULane and Tusimple datasets, while for FoggyLane, we extended the training epochs to ensure reliable results

5.4. Quantitative Results

5.4.1. Results on FoggyLane

We evaluated our proposed method on the FoggyLane dataset and compared it with other leading lane detection methods. As shown in the Tabel 2, we mainly compared the methods in terms of F1 scores, computational complexity (GFlops), processing speed (FPS).

From the Table 2, it is evident that our method achieves state-of-the-art performance on the foggy lane detection dataset FoggyLane, with F1@50, F1@65, F1@75, and F1@85 scores of 95.04, 88.61, 77.32, and 45.02, respectively. These results surpass the best-performing alternative methods by margins of 2.95%, 4.63%, 5.17%, and 3.41%. The mean F1 (mF1) score demonstrates a 3.32% improvement over the strongest competing approach. Notably, the SwinGFFM-t variant achieves an F1@50 score of 92.34, which even exceeds the performance of DLA34-based CLRNet, pre-

Table 4: Comparison with Advanced Lane Detection on FoggyTusimple dataset.

Method	Venue	Backbone	F1(%)	ACC(%)	FP(%)	FN(%)
SCNN(Pan et al., 2018)	AAAI 2018	VGG16	94.64	95.89	5.87	4.78
UFLD(Qin et al., 2020)	ECCV 2020	ResNet18	94.57	93.60	3.49	7.59
UFLD(Qin et al., 2020)	ECCV 2020	ResNet34	95.05	95.10	4.84	5.08
LaneATT(Tabelini et al., 2021a)	CVPR 2020	ResNet18	95.77	95.78	3.83	3.53
LaneATT(Tabelini et al., 2021a)	CVPR 2020	ResNet34	96.15	95.50	4.59	3.06
LSTR(Liu et al., 2021b)	WACV 2021	ResNet34	94.70	95.58	5.74	4.81
RESA(Zheng et al., 2021)	AAAI 2021	ResNet34	95.22	95.60	4.63	4.95
RESA(Zheng et al., 2021)	AAAI 2021	ResNet50	95.51	95.83	4.53	4.43
CondLane(Liu et al., 2021a)	JCCV 2021	ResNet18	95.41	94.81	3.80	5.46
CondLane(Liu et al., 2021a)	JCCV 2021	ResNet34	95.65	94.69	3.63	5.13
CLRNet(Zheng et al., 2022)	CVPR 2022	ResNet18	96.48	95.64	3.89	3.11
CLRNet(Zheng et al., 2022)	CVPR 2022	ResNet34	96.23	95.94	4.34	3.17
FLAMNet(Ran et al., 2023)	IEEE TITS 2023	ResNet18	96.52	95.65	3.84	3.09
FLAMNet(Ran et al., 2023)	IEEE TITS 2023	ResNet101	96.34	95.98	4.45	2.82
DBNet(Dai et al., 2024)	IEEE TIV 2024	ResNet18	95.71	93.89	3.53	5.12
DBNet(Dai et al., 2024)	IEEE TIV 2024	ResNet34	95.61	93.72	3.48	5.38
HWLane(Zhao et al., 2024)	IEEE TITS 2024	Res34	95.54	95.91	4.32	4.60
PolarRCNN(Wang et al., 2025)	IEEE TITS 2025	ResNet34	96.33	95.91	4.50	2.77
PolarRCNN(Wang et al., 2025)	IEEE TITS 2025	DLA34	96.37	94.99	3.21	4.09
Ours	-	SwinGFFM-t	96.63	95.86	2.77	4.04
Ours	-	SwinGFFM-s	96.95(0.43)	96.10(0.12)	2.32(0.89)	3.83

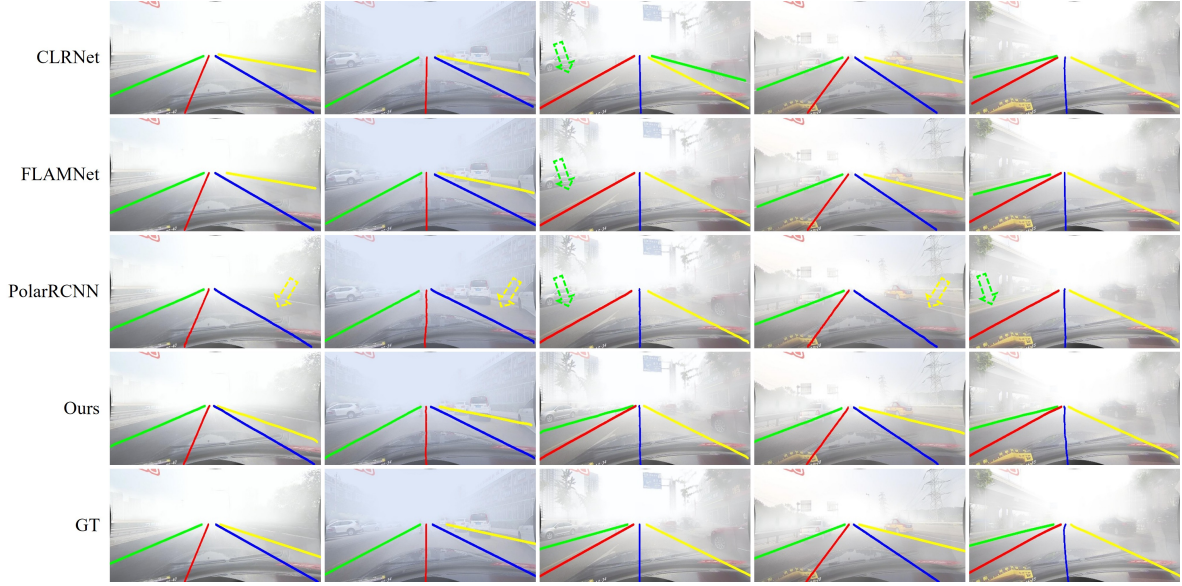


Figure 12: Visualization results of CLRNet(Zheng et al., 2022), FLAMNet(Ran et al., 2023), PolarRCNN(Wang et al., 2025) and our method on FoggyCULane testing set. The arrows indicate instances of lane lines that were not correctly detected by the corresponding method.

viously the top-performing method among comparative approaches.

5.4.2. Results on FoggyCULane

We compared our method with other advanced lane detection methods on the FoggyCULane dataset. As shown in the Table 3, our method consistently achieved the best performance across various scenarios. Additionally, our model achieved the highest overall F1 score of 79.85, which achieves a 0.72% improvement over the best alternative method.

5.4.3. Results on FoggyTusimple

As shown in the Table 4, the traffic scenes in the FoggyTusimple dataset are relatively simple, resulting in smaller performance differences between methods. Nonetheless, our method achieved an F1 score of 96.95, outperforming the best existing method by 0.43%. This further demonstrates the effectiveness of our method in foggy conditions.

5.5. Ablation Study

We conducted ablation studies on the FoggyLane and FoggyCULane datasets to evaluate the effectiveness of the GFFM, KFFM, and LEEM modules, using Swin-t as the backbone. As shown in Tables 5 and 6, each module improves the model’s performance. The GFFM module contributes the most, increasing the F1-score by 1.07 on FoggyLane and 0.41 on FoggyCULane, highlighting

Table 5: Ablation experiments of different components on the FoggyLane dataset.

Model	GFFM	KFFM	LEEM	F1-score	Gflops(G)
Baseline				90.36	13.77
	✓			91.43	11.94
	✓	✓		92.06	11.97
Ours	✓	✓	✓	92.34↑	12.01

its ability to capture both local and global information. Adding the KFFM module further boosts the F1-score by 0.63 on FoggyLane and 0.26 on FoggyCULane. Finally, the LEEM module improves edge detection, increasing the F1-score by 0.28 on FoggyLane and 0.14 on FoggyCULane.

5.6. Model deployment

To further evaluate the performance of our algorithm in real-world scenarios, in addition to experiments on existing datasets, we also deployed and tested the model on the vehicle. Specifically, we implemented an edge computing system on the vehicle, as illustrated in the Fig. 14. This system comprises the NVIDIA Jetson AGX Orin edge computing device, a monitor, a camera, and a power supply unit. The results of the evaluation demonstrate that our approach can operate in real-time with high accuracy on the vehicle’s edge comput-

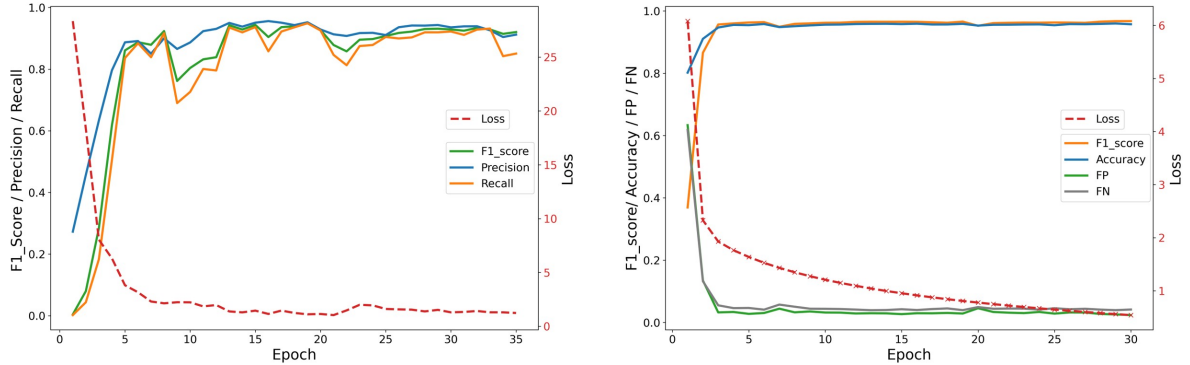


Figure 13: Several metrics of our model’s performance during the training process on the FoggyLane and FoggyTusimple datasets, with results on FoggyLane on the left and FoggyTusimple on the right.



Figure 14: A edge computing system built with NVIDIA Jetson AGX Orin. After experimental validation, it has been demonstrated that our method can run accurately on the vehicle’s edge computing platform with limited computational resources, achieving a performance of 38.4 FPS.

ing platform, despite the constraints on computational resources.

Table 6: Ablation experiments of different components on the Foggy-CULane dataset.

Model	GFFM	KFFM	LEEM	F1-score	Gflops(G)
Baseline				77.85	13.77
	✓			78.26	11.94
	✓	✓		78.52	11.97
Ours	✓	✓	✓	78.66↑	12.01

6. Conclusion

This study focuses on lane detection in foggy conditions, aiming to address the range of challenges posed by foggy environments, which is crucial for ensuring

driving safety in fog and enhancing Advanced Driver Assistance System (ADAS) capabilities. To address the current lack of publicly available datasets for lane detection in foggy conditions, we constructed a real-world foggy lane dataset, FoggyLane, and synthesized two additional foggy datasets, FoggyCULane and FoggyTusimple, based on the popular CULane and Tusimple datasets.

In response to the challenges of lane detection in foggy scenarios, we propose an end-to-end fog-enhanced lane detection method. First, this method incorporates a Global Feature Fusion Module in the backbone network to address the absence of global spatial information in foggy scenes. Second, we employ a dynamic convolution-based detection head for instance-sensitive lane segmentation, integrating a Kernel Feature Fusion Module within the detection head to automatically capture associations between lane instances. Additionally, a Low-Level Edge Enhancement Module

was added to increase the network's focus on edge information, mitigating the loss of edge details and improving lane detection accuracy under foggy conditions.

Comparative experiments on the FoggyLane, Foggy-CULane, and FoggyTusimple datasets with other advanced lane detection methods demonstrate that our approach achieves superior performance in both clear and foggy conditions, significantly improving lane detection accuracy. Furthermore, with TensorRT acceleration, our method achieves an inference speed of 38.4 FPS on the NVIDIA Jetson AGX Orin, further validating its practical applicability in real-world scenarios.

Acknowledgement

This project is jointly supported by National Natural Science Foundation of China (Nos. 52172350, W2421069 and 51775565), the Guangdong Basic and Applied Research Foundation (No. 2022B1515120072), the Guangzhou Science and Technology Plan Project (No. 2024B01W0079), the Nansha Key RD Program (No. 2022ZD014), the Science and Technology Planning Project of Guangdong Province (No. 2023B1212060029). **We would like to release our source code and dataset.**

References

- Abualsaud, H., Liu, S., Lu, D.B., Situ, K., Rangesh, A., Trivedi, M.M., 2021. Laneaf: Robust multi-lane detection with affinity fields. *IEEE Robotics and Automation Letters* 6, 7477–7484. doi:10.1109/LRA.2021.3098066.
- Alshakhs, A., Mysorewala, M., Nasir, A., 2025. Coordinated multi lane-changing on highways for connected and automated vehicles in mixed traffic. *Expert Systems with Applications* 286, 127890. doi:https://doi.org/10.1016/j.eswa.2025.127890.
- Aly, M., 2008. Real time detection of lane markers in urban streets, in: 2008 IEEE Intelligent Vehicles Symposium (IV), pp. 7–12. doi:10.1109/IVS.2008.4621152.
- Awan, M., Whangbo, T.K., Shin, J., 2025. Deep learning methods for autonomous driving scene understanding tasks: A review. *Expert Systems with Applications* 287, 128098. doi:https://doi.org/10.1016/j.eswa.2025.128098.
- Behrendt, K., Soussan, R., 2019. Unsupervised labeled lane markers using maps, in: Proceedings of the IEEE/CVF International Conference on Computer Vision Workshops, pp. 832–839. doi:10.1109/ICCVW.2019.00111.
- Chen, J., Zhao, N., Zhang, R., Chen, L., Huang, K., Qiu, Z., 2023. Refined crack detection via lecsformer for autonomous road inspection vehicles. *IEEE Transactions on Intelligent Vehicles* 8, 2049–2061. doi:10.1109/TIV.2022.3204583.
- Chen, X., Wang, Y., Chen, X., Zeng, W., 2021. S2r-depthnet: Learning a generalizable depth-specific structural representation, in: Proceedings of the IEEE/CVF Conference on Computer Vision and Pattern Recognition, pp. 3034–3043. doi:10.1109/CVPR46437.2021.00305.
- Chen, Y., Li, W., Sakaridis, C., Dai, D., Van Gool, L., 2018. Domain adaptive faster r-cnn for object detection in the wild, in: Proceedings of the IEEE Conference on Computer Vision and Pattern Recognition, pp. 3339–3348. doi:10.1109/CVPR.2018.00352.
- Chen, Z., Liu, Q., Lian, C., 2019. Pointlanenet: Efficient end-to-end cnns for accurate real-time lane detection, in: 2019 IEEE Intelligent Vehicles Symposium (IV), pp. 2563–2568. doi:10.1109/IVS.2019.8813778.
- Chen, Z., Zhang, Z., Su, Q., Yang, K., Wu, Y., He, L., Tang, X., 2026. Object detection for autonomous vehicles under adverse weather conditions. *Expert Systems with Applications* 296, 128994. doi:https://doi.org/10.1016/j.eswa.2025.128994.
- Dai, X., Xie, J., Zhang, G., Chang, K., Chen, F., Wang, Z., Tang, C., 2024. Dbnet: A curve-based dynamic association framework for lane detection. *IEEE Transactions on Intelligent Vehicles* doi:10.1109/TIV.2024.3370213.
- Dong, X., Bao, J., Chen, D., Zhang, W., Yu, N., Yuan, L., Chen, D., Guo, B., 2022. Cswin transformer: A general vision transformer backbone with cross-shaped windows, in: Proceedings of the IEEE/CVF Conference on Computer Vision and Pattern Recognition, pp. 12124–12134. doi:10.1109/CVPR52688.2022.01181.
- Farhadi, A., Redmon, J., 2018. Yolov3: An incremental improvement. *arXiv preprint arXiv:1804.02767*, 1–6. doi:10.48550/arXiv.1804.02767.
- GoogleMaps, Accessed: 2024. <https://www.google.com/maps>.
- Harald, K., 1924. Theorie der horizontalen sichtweite: Kontrast und sichtweite. *Keim und Nemnich, Munich* 12, 33–53. doi:10.1007/978-3-663-04661-5_2.
- He, K., Sun, J., Tang, X., 2011. Single image haze removal using dark channel prior. *IEEE Transactions on Pattern Analysis and Machine Intelligence* 33, 2341–2353. doi:10.1109/TPAMI.2010.168.
- Hnewa, M., Radha, H., 2021. Multiscale domain adaptive yolo for cross-domain object detection, in: Proceedings of the IEEE International Conference on Image Processing, pp. 3323–3327. doi:10.1109/ICIP42928.2021.9506039.
- Hou, C., Hou, J., Yu, C., 2016. An efficient lane markings detection and tracking method based on vanishing point constraints, in: Chinese Control Conference (CCC), IEEE. pp. 6999–7004. doi:10.1109/ChiCC.2016.7554460.
- Huang, S.C., Le, T.H., Jaw, D.W., 2020. Dsnet: Joint semantic learning for object detection in inclement weather conditions. *IEEE Transactions on Pattern Analysis and Machine Intelligence* 43, 2623–2633. doi:10.1109/TPAMI.2020.2977911.
- Huang, X., Cheng, X., Geng, Q., Cao, B., Zhou, D., Wang, P., Lin, Y., Yang, R., 2018. The apollo-scape dataset for autonomous driving, in: Proceedings of the IEEE Conference on Computer Vision and Pattern Recognition Workshops, pp. 954–960. doi:10.1109/CVPRW.2018.00141.
- Li, J., Xu, R., Ma, J., Zou, Q., Ma, J., Yu, H., 2023. Domain adaptive object detection for autonomous driving under foggy weather, in: Proceedings of the IEEE/CVF Winter Conference on Applications of Computer Vision, pp. 612–622.
- Li, X., Li, J., Hu, X., Yang, J., 2019. Line-cnn: End-to-end traffic line detection with line proposal unit. *IEEE Transactions on Intelligent Transportation Systems* 21, 248–258. doi:10.1109/TITS.2019.2890870.
- Liu, L., Chen, X., Zhu, S., Tan, P., 2021a. Condlanenet: A top-to-down lane detection framework based on conditional convolution, in: Proceedings of the IEEE/CVF International Conference on Computer Vision, pp. 3773–3782. doi:10.1109/ICCV48922.2021.00375.
- Liu, R., Yuan, Z., Liu, T., Xiong, Z., 2021b. End-to-end lane shape prediction with transformers, in: Proceedings of the IEEE/CVF Winter Conference on Applications of Computer Vision, pp. 3694–3702. doi:10.1109/WACV48630.2021.00374.

- Liu, Z., Hu, H., Lin, Y., Yao, Z., Xie, Z., Wei, Y., Ning, J., Cao, Y., Zhang, Z., Dong, L., et al., 2022. Swin transformer v2: Scaling up capacity and resolution, in: Proceedings of the IEEE/CVF Conference on Computer Vision and Pattern Recognition, pp. 12009–12019. doi:10.1109/CVPR52688.2022.01170.
- Liu, Z., Lin, Y., Cao, Y., Hu, H., Wei, Y., Zhang, Z., Lin, S., Guo, B., 2021c. Swin transformer: Hierarchical vision transformer using shifted windows, in: Proceedings of the IEEE/CVF International Conference on Computer Vision, pp. 10012–10022. doi:10.1109/ICCV48922.2021.00986.
- Neven, D., De Brabandere, B., Georgoulis, S., Proesmans, M., Van Gool, L., 2018. Towards end-to-end lane detection: an instance segmentation approach, in: 2018 IEEE Intelligent Vehicles Symposium (IV), IEEE. pp. 286–291. doi:10.1109/IVS.2018.8500547.
- Nie, X., Xu, Z., Zhang, W., Dong, X., Liu, N., Chen, Y., 2022. Foggy lane dataset synthesized from monocular images for lane detection algorithms. *Sensors* 22, 5210. doi:10.3390/s22145210.
- Pan, X., Shi, J., Luo, P., Wang, X., Tang, X., 2018. Spatial as deep: Spatial cnn for traffic scene understanding, in: Proceedings of the AAAI Conference on Artificial Intelligence.
- Pexels, 2025. <https://www.pexels.com/zh-cn/>.
- Preeti, Rana, C., 2024. Artificial intelligence based object detection and traffic prediction by autonomous vehicles – a review. *Expert Systems with Applications* 255, 124664. doi:https://doi.org/10.1016/j.eswa.2024.124664.
- Qin, Z., Wang, H., Li, X., 2020. Ultra fast structure-aware deep lane detection, in: European Conference on Computer Vision, Springer. pp. 276–291. doi:10.1007/978-3-030-58586-0_17.
- Ran, H., Yin, Y., Huang, F., Bao, X., 2023. Flamnet: A flexible line anchor mechanism network for lane detection. *IEEE Transactions on Intelligent Transportation Systems* 24, 12767–12778. doi:doi:10.1109/TITS.2023.3290991.
- Redmon, J., 2016. You only look once: Unified, real-time object detection, in: Proceedings of the IEEE Conference on Computer Vision and Pattern Recognition, pp. 779–788. doi:10.1109/CVPR.2016.91.
- Sang, I.C., Norris, W.R., 2025. Improved generalizability of cnn based lane detection in challenging weather using adaptive pre-processing parameter tuning. *Expert Systems with Applications* 275, 127055. doi:https://doi.org/10.1016/j.eswa.2025.127055.
- Shunmuga Perumal, P., Wang, Y., Sujasree, M., Tulshain, S., Bhutani, S., Suriyah, M.K., Kumar Raju, V.U., 2023. Lanescannet: A deep-learning approach for simultaneous detection of obstacle-lane states for autonomous driving systems. *Expert Systems with Applications* 233, 120970. doi:https://doi.org/10.1016/j.eswa.2023.120970.
- Son, J., Yoo, H., Kim, S., Sohn, K., 2015. Real-time illumination invariant lane detection for lane departure warning system. *Expert Systems with Applications* 42, 1816–1824. doi:https://doi.org/10.1016/j.eswa.2014.10.024.
- Tabelini, L., Berriel, R., Paixao, T.M., Badue, C., De Souza, A.F., Oliveira-Santos, T., 2021a. Keep your eyes on the lane: Real-time attention-guided lane detection, in: Proceedings of the IEEE/CVF Conference on Computer Vision and Pattern Recognition, pp. 294–302. doi:10.1109/CVPR46437.2021.00036.
- Tabelini, L., Berriel, R., Paixao, T.M., Badue, C., De Souza, A.F., Oliveira-Santos, T., 2021b. Polylnenet: Lane estimation via deep polynomial regression, in: Proceedings of the IEEE International Conference on Pattern Recognition, IEEE. pp. 6150–6156. doi:10.1109/ICPR48806.2021.9412265.
- Tian, Z., Zhang, B., Chen, H., Shen, C., 2023. Instance and panoptic segmentation using conditional convolutions. *IEEE Transactions on Pattern Analysis and Machine Intelligence* 45, 669–680. doi:10.1109/TPAMI.2022.3145407.
- Tusimple, 2017. <https://github.com/TuSimple/tusimple-benchmark>.
- Wang, J., Sun, K., Cheng, T., Jiang, B., Deng, C., Zhao, Y., Liu, D., Mu, Y., Tan, M., Wang, X., Liu, W., Xiao, B., 2021. Deep high-resolution representation learning for visual recognition. *IEEE Transactions on Pattern Analysis and Machine Intelligence* 43, 3349–3364. doi:10.1109/TPAMI.2020.2983686.
- Wang, S., Liu, J., Cao, X., Song, Z., Sun, K., 2025. Polar r-cnn: End-to-end lane detection with fewer anchors. *IEEE Transactions on Intelligent Transportation Systems*, 1–13doi:10.1109/TITS.2025.3564979.
- Xu, H., Wang, S., Cai, X., Zhang, W., Liang, X., Li, Z., 2020. Curvelane-nas: Unifying lane-sensitive architecture search and adaptive point blending, in: European Conference on Computer Vision, Springer. pp. 689–704. doi:10.1007/978-3-030-58555-6_41.
- Yoo, S., Lee, H.S., Myeong, H., Yun, S., Park, H., Cho, J., Kim, D.H., 2020. End-to-end lane marker detection via row-wise classification, in: Proceedings of the IEEE/CVF Conference on Computer Vision and Pattern Recognition Workshops, pp. 1006–1007. doi:10.1109/CVPRW50498.2020.00511.
- YouTube, Accessed: 2024. <https://www.youtube.com/>.
- Yu, F., Chen, H., Wang, X., Xian, W., Chen, Y., Liu, F., Madhavan, V., Darrell, T., 2020. Bdd100k: A diverse driving dataset for heterogeneous multitask learning, in: Proceedings of the IEEE/CVF Conference on Computer Vision and Pattern Recognition, pp. 2636–2645. doi:10.1109/CVPR42600.2020.00271.
- Yu, F., Wang, D., Shelhamer, E., Darrell, T., 2018. Deep layer aggregation, in: Proceedings of the IEEE Conference on Computer Vision and Pattern Recognition, pp. 2403–2412. doi:10.1109/CVPR.2018.00255.
- Zhang, R., Peng, J., Gou, W., Ma, Y., Chen, J., Hu, H., Li, W., Yin, G., Li, Z., 2024a. A robust and real-time lane detection method in low-light scenarios to advanced driver assistance systems. *Expert Systems with Applications* 256, 124923. doi:10.1016/j.eswa.2024.124923.
- Zhang, R., Yang, S., Lyu, D., Wang, Z., Chen, J., Ren, Y., Gao, B., Lv, Z., 2025. Agsenet: A robust road ponding detection method for proactive traffic safety. *IEEE Transactions on Intelligent Transportation Systems* 26, 497–516. doi:10.1109/TITS.2024.3506659.
- Zhang, S., Tuo, H., Hu, J., Jing, Z., 2021. Domain adaptive yolo for one-stage cross-domain detection, in: Asian Conference on Machine Learning, PMLR. pp. 785–797.
- Zhang, X., Zhu, X., 2019. Autonomous path tracking control of intelligent electric vehicles based on lane detection and optimal preview method. *Expert Systems with Applications* 121, 38–48. doi:https://doi.org/10.1016/j.eswa.2018.12.005.
- Zhang, Y., Zheng, Y., Tu, Z., Wu, C., Zhang, T., 2024b. Cffm: Multi-task lane object detection method based on cross-layer feature fusion. *Expert Systems with Applications* 257, 125051. doi:https://doi.org/10.1016/j.eswa.2024.125051.
- Zhao, J., Qiu, Z., Hu, H., Sun, S., 2024. Hwlane: Hw-transformer for lane detection. *IEEE Transactions on Intelligent Transportation Systems* 25, 9321–9331. doi:10.1109/TITS.2024.3386531.
- Zheng, T., Fang, H., Zhang, Y., Tang, W., Yang, Z., Liu, H., Cai, D., 2021. Resa: Recurrent feature-shift aggregator for lane detection, in: Proceedings of the AAAI Conference on Artificial Intelligence, pp. 3547–3554. doi:10.1609/aaai.v35i4.16469.
- Zheng, T., Huang, Y., Liu, Y., Tang, W., Yang, Z., Cai, D., He, X., 2022. Clrnet: Cross layer refinement network for lane detection, in: Proceedings of the IEEE/CVF Conference on Computer Vision and Pattern Recognition, pp. 898–907. doi:10.1109/CVPR52688.2022.00097.